Mechanics of Advanced Composite Structures 9 (2022) 263 – 274

Semnan University

Mechanics of Advanced Composite Structures

journal homepage: http://MACS.journals.semnan.ac.ir

Finite Element Analysis of Mechanical Properties of Basalt-Carbon Epoxy Hybrid Laminates

A. A. Pradhan[a], A. M. Kotasthane[a], A. A. Shaikh[a], S. Patil[a*], S. Karuppanan[b]

[a] *Department of Mechanical Engineering, Manipal University Jaipur, Dehmi Kalan, 303007, Jaipur, Rajasthan, India*
[b] *Department of Mechanical Engineering, Universiti Teknologi PETRONAS, 32610 Bandar Seri Iskandar, Perak, Malaysia*

KEYWORDS

Finite Element Analysis;
Tsai-Wu failure;
Hybrid composites;
Basalt fibre;
Carbon fibre.

ABSTRACT

Hybrid laminates have been utilized in vast applications, namely aircraft, automotive, and other areas of light weight and high strength requirement. There are various types of hybrid laminates and an assessment of these laminates for their application is necessary. Experimental testing as per ASTM is expensive since it is destructive testing. In addition, the hybridization of basalt, a promising fibre along with other fibres has shown better laminate properties. Basalt-carbon epoxy hybrid laminated composites are a comparably inexpensive and sustainable alternative to conventional carbon fibre epoxy composites. Thus, in this paper, the evaluation of the new and advanced basalt-carbon epoxy hybrid laminated composites under static loading was conducted using Finite Element Analysis. Mechanical properties of basalt-carbon epoxy hybrid laminated composites such as tensile and compression strength, flexure strength, interlaminar, and in-plane shear strength were evaluated through different static test simulations. Specimens having different stack-up sequences and fibre orientations were analysed for failure based on Tsai-Wu failure criteria using commercial finite element software ANSYS Composite Pre-Post (ACP) and ANSYS Mechanical. The outcome of this work shows that laminates with basalt fibres on the inner side and carbon fibres on the outer side provided a better alternative with around 90-98% equivalent strength to pure carbon laminates in various mechanical strength tests. In addition, the lay-up of specimen C2 $[0_2C/\pm45B/0B]_S$ was found to be the optimal stacking arrangement. Using specimen C2 as a substitute to pure carbon fibre laminate not only provides almost equivalent strength but also reduces the cost by up to 40%. The comparable strength property of specimen C2 was due to the placement of 0^o carbon fibre at the outer faces of the composite.

1. Introduction

Composite materials are constructed using two, or more materials (known as constituents) that have varying characteristics, schematically represented in Figure 1. Composite materials exhibit characteristics derived from each of the individual constituents. However, the constituents remain distinct and isolated within the final structure. The characteristics of the new material are dependent on the individual constituents as well as the way the constituents are combined. The resulting properties can exceed or possess the combined properties of the individual constituents.

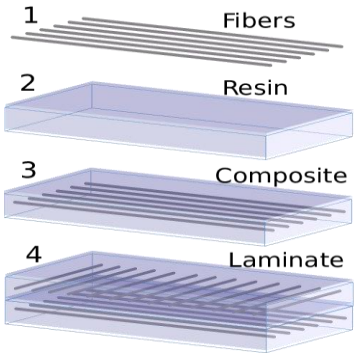

Figure 1: Schematic representation of a composite laminate.

* Corresponding author. Tel.: +91-141-3999100 Ext. 610
E-mail address: santosh045@gmail.com

DOI: 10.22075/macs.2022.25300.1370
Received 21-11-20; Received in revised form 22-06-21; Accepted 22-08-05

In recent years, it has been observed that basalt fibre finds a spectrum of applications. Wang et al. [1] evaluated the damage characteristics of basalt fibre reinforced mortar under compression. Their results showed that the addition of basalt fibre improved the rigidity and the ductility of the mortar specimen. Evaluation of mechanical properties and degradation of basalt was carried out by Sakthivel et al. [2]. Their work showed that basalt fibre reinforced polypropylene (BFRP) is superior to glass fibre reinforced polypropylene (GFRP). Some researchers claim that basalt fibre has a good potential to provide benefits that are superior to glass fibre, and significantly cost-effective to carbon fibre. Basalt fibre has received increasing attention as a newcomer to fibre reinforced polymers based on its superior mechanical properties like high tensile strength, modulus, rupture strength, good range of thermal performance, good chemical resistance, superior electromagnetic properties, good resistance to vibration, high compressive strength, and better strain to failure, inexpensive, environmentally and ecologically harmless based on the investigations by Parnas et al. [3] as well as Singha [4]. Basalt is the most abundant rock type in the earth's crust. Basalt fibre is made from extremely fine fibres composed of the mineral's plagioclase, pyroxene, and olivine. Due to its extraordinary mechanical properties, basalt fibre is seen as a potential alternative to S2-fibreglass and E-glass which have already established a benchmark in the industry.

Mingchao et al. [5] investigated the mechanical properties of basalt fibre reinforced plastic. They concluded that the interface formed between basalt fibre reinforced plastic and epoxy resin is better than glass fibre reinforced plastic. Czigany et al. [6] examined the basalt fibre as a reinforcement of polymer composites. They claimed that basalt fibre due to its outstanding mechanical properties can be an alternative to glass fibre. Aslan et al. [7] used basalt fibre in conjunction with graphene nanoplatelets and subjected it to tensile, flexural, and impact loads. Their work was indicative of superior flexural properties of basalt fibre as well as the finding that the ratio of basalt fibre content increased the impact energy of hybrid composites. Khalili et al. [8] presented an experimental investigation on the mechanical behaviour of basalt fibre reinforced composite under tensile and bending loads. The results revealed that basalt fibres can be successfully used instead of glass fibres in fibre composite manufacturing. Hawileh et al. [9] presented an experimental and analytical investigation on the behaviour of reinforced concrete beams strengthened in flexure properties by means of a different combination of externally bonded hybrid Glass and Carbon Fibre Reinforced Polymer (GFRP/CFRP) sheets.

Naser et al. [10] presented an application of FRP systems in reinforced concrete structural members and highlighted the performance of FRPs under extreme conditions such as elevated temperature, saline environment, and cycles of freezing and thawing. Maxineasa et al. [11] conducted life cycle assessment studies to determine if composite materials should be considered in the life cycle analysis of strengthening concrete beams with fibre reinforced plastics where basalt fibre was explored to minimize the environmental footprint. Refai et al. [12] reported on the experimental and analytical investigation of the shear performance of concrete beams cast with basalt fibre-reinforced concrete and a good agreement between the predicted and experimental shear strength was evident. Gencel et al. [13] studied and reported the addition of basalt fibre which then enhances mechanical properties while increasing the porosity and water absorption values of foam concrete.

Yang et al. [14] studied the effects of raw material homogenization on the structure of basalt melt and the performance of fibres. They concluded that fibre strength increased with increasing degree of polymerization. As the homogenization time and temperature increased, coefficients of variation of fibre strength and fibre diameter decreased, indicating enhanced fibre stability. Zheng et al. [15] explored Nano-SiO2 modified basalt fibre for enhancing the mechanical properties of oil well cement. Their results indicate that nano-silica on the surface of basalt fibres can improve the bond strength between the fibres and the cement matrix, thus enhancing the bridging effect of basalt fibres in the cement matrix. Chandrasekar et al. [16] explored the low-velocity impact properties of basalt fibre-reinforced composites, as they have the potential to be applied in aeronautical applications where low-velocity impact damage occurs due to bird strikes, hailstones, runway debris, etc. They concluded that the impact properties of these composites can be tailored by using different fibre architecture, hybridization, varying the impact energy, impact velocity, and sample temperature. Basalt/Carbon experimentations for wind turbine blade application conducted by Mengal et al. [17] can be considered for validation of the FEA analysis conducted in this work. There has been a great interest in hybrid materials, particularly with the combination of basalt fibre and carbon fibre as can be seen from this work. Due to its extraordinary mechanical properties over other fibre reinforced composites, its use in wind turbine blades is ideal.

Due to the ever-increasing demand and methods of manufacturing, the cost of carbon fibre presents an unprecedented economic situation. This is where basalt fibre plays a pivotal role as it is both, abundant and inexpensive. Ludovico et al. [18] presented a paper where basalt fibre is found to be cheaper compared to carbon and glass fibres due to less processing and energy consumption during its manufacturing process. Due to different fibre manufacturing methods and specifications, a fixed cost could not be estimated. Our findings after consulting several manufacturers led us to establish the average cost of unidirectional carbon fibre as USD 26.92 per m^2 and the cost of unidirectional basalt fibre as USD 16.15 per m^2. For accounting for regional variation in the manufacturing cost of the fibres, the average of five different costs from five vendors was considered for this work. Substituting basalt layers in the place of carbon fibre is expected to provide a strength which is second only to pure carbon fibre while offering significant cost reduction. As per literature [11][18], basalt fibre has been found to be inexpensive compared to carbon fibre due to a simpler fibre manufacturing process. Basalt products have no toxic reaction with air or water and are non-combustible and explosion-proof. Thus, basalt fibre can be classified as a sustainable material [19]. In continuation, the following are the major objectives of this work:

1. To evaluate the ultimate tensile strength, ultimate compressive strength, ultimate flexural strength, interlaminar shear strength, and in-plane shear strength of basalt-carbon epoxy hybrid laminated composite based on Tsai-Wu failure index parameters using FEA.

2. To propose an optimal stacking sequence for basalt/carbon hybrid laminates based on comparative strength analysis.

3. To estimate cost reduction from using basalt in a 4:4 ratio with carbon fibre with that of pure carbon reference specimen C1.

Tsai-Wu criterion is deemed fit as it considers the total strain energy which includes both distortion energy and dilatation energy for predicting failure. In comparison to Tsai-Hill failure, Tsai Wu's criteria is more general as it distinguishes between compressive and tensile failure strengths.

2. Materials and Methodology

2.1. Materials

Materials used for the hybrid laminates were carbon fibre, basalt fibre, and resin LY556 as the matrix. Six symmetrical lamination stacking sequences with eight layers of unidirectional 0° and biaxial +45° were selected for the current study. One eight-layered unidirectional 0° fibre layup of pure carbon fibre and one eight-layered unidirectional 0° fibre layup of pure basalt were used as a reference. For all six hybrid composite laminates, the composition of basalt to carbon fibre ratio was maintained at 4:4 with varying stacking sequences. Table 1 lists the stacking sequence arrangement of coupon specimens and fibre orientations.

Table 1: Stack up sequence [17].

Group	Laminate Code	Stacking Sequence	Fibre Orientation (°)
Pure laminates	C1	C_8	$[0_8C]$
	B1	B_8	$[0_8B]$
Hybrid laminates with carbon fibres at the outer layers	C2	$C_2B_4C_2$	$[0_2C/\pm45B/0B]_S$
	C3	$C_2B_4C_2$	$[0_2C/0B/\pm45B]_S$
	C4	$C_2B_4C_2$	$[0_2C/\pm45_2B]_S$
Hybrid laminates with basalt fibres at the outer layers	B2	$B_2C_4B_2$	$[0B/\pm45B/0_2C]_S$
	B3	$B_2C_4B_2$	$[\pm45B/0B/0_2C]_S$
	B4	$B_2C_4B_2$	$[\pm45_2B/0_2C]_S$

Table 2: Combined material properties of matrix and fibres [16]

Properties	Basalt + Epoxy	Carbon + Epoxy
Density (kg/m^3)	1830	1560
Young's Modulus in X-direction (MPa)	38900	103000
Young's Modulus in Y-direction (MPa)	7470	8019.02
Young's Modulus in Z-direction (MPa)	7470	8019.02
Poisson's Ratio XY	0.281	0.3447
Poisson's Ratio YZ	0.455	0.3447
Poisson's Ratio XZ	0.281	0.4247
Shear Modulus XY (MPa)	2710	3298
Shear Modulus YZ (MPa)	2540	3298
Shear Modulus XZ (MPa)	2710	2814
Tensile strength in X-direction (MPa)	1220	3200
Tensile strength in Y-direction (MPa)	62.1	70
Tensile strength in Z-direction (MPa)	62.1	70
Compressive strength in X-direction (MPa)	-780	-918
Compressive strength in Y-direction (MPa)	-93.1	-170
Compressive strength in Z-direction (MPa)	-93.1	-170
Shear strength in XY direction (MPa)	85.7	88
Shear strength in YZ direction (MPa)	51.42	50
Shear strength in XZ direction (MPa)	85.7	88

The coupling coefficient for Tsai-Wu failure of all materials is -1. Orthotropic strain limits can be calculated using the relation in Eq. 1.

$$Modulus\ of\ Elasticity = \frac{Orthotropic\ Stress}{Orthotropic\ Strain} \quad \text{(Eq. 1)}$$

2.2. Specimen Geometries

The specimens for the mechanical tests were designed according to the ASTM standards - ASTM D3039 [21] for tensile test, ASTM D6641 [22] for compression test, ASTM D7078 [23] for flexural fest, ASTM D2344 [24] for interlaminar test, and ASTM D7264 [25] for in-plane shear test. The specimen dimensions are as in Figures 2-4.

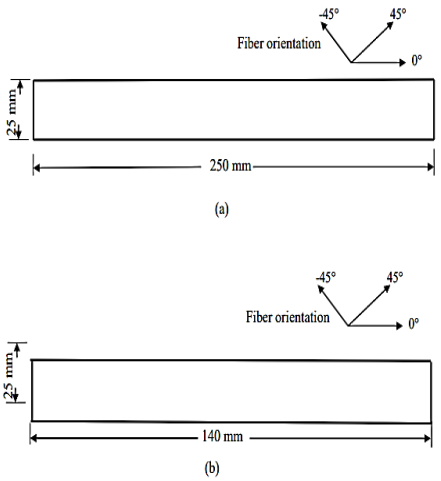

Figure 2: (a) Tensile Specimen [17] (b) Compression Specimen [18].

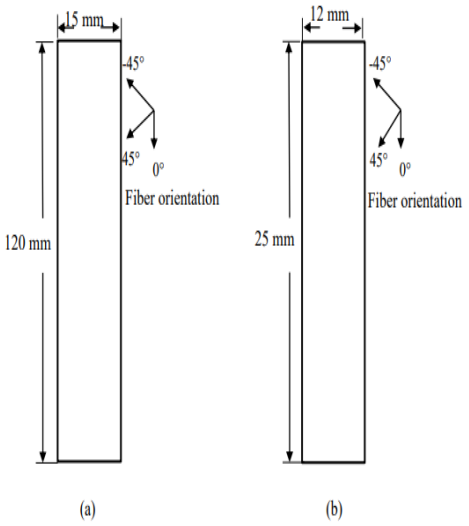

Figure 3: (a) Flexural specimen [19] (b) Interlaminar specimen [20].

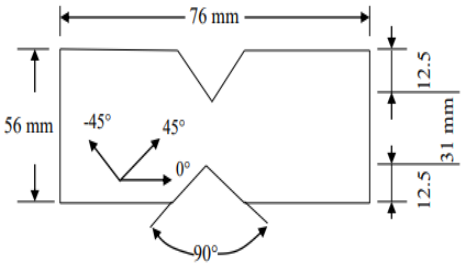

Figure 4: In-plane shear specimen [21]

2.3. Methodology

In ANSYS Workbench [27], all material data mentioned in Table 2 served as the input for the Engineering Data module in ANSYS Workbench as shown in Figure 5. After the input of material data, the design modeler was used to draft the specimen geometry. Then the model was meshed in ANSYS Mechanical. The mesh size was selected from a range of 0.5 to 1 mm depending on the specimen geometry indicated in Figures 2-4. The meshed model was then exported into ANSYS ACP-Pre for modeling, material assignment, fibre orientation, and stacking of layers. Each layer was assigned material, fibre direction, and stack-up sequence according to the specimen configurations as mentioned in Table 1. A thickness of 0.4 mm was assigned to each layer of the composite model which makes the solid composite model 3.2 mm thick. A schematic of the solid composite model demonstrating the fibre orientation of 45° with green arrows and 0° reference fibre direction with yellow arrows is shown in Figure 6. The meshed solid composite model was transferred from ANSYS ACP to ANSYS Mechanical/ Static Structural for the application of loading and boundary conditions. As per the literature [17], the tests were displacement controlled. Displacement was applied as a function of time-steps which can be input by changing the solver analysis settings in ANSYS. The steps required vary for each test and the time required to achieve failure can also be evaluated as shown in Figure 7. Double displacement at 1 mm/min was levied on the side faces of the meshed model as shown in Figure 8. The solution was then exported to ACP-Post. The Tsai-Wu failure criteria was selected and equivalent von-Mises stress and shear stress were evaluated. The composite model fails when the Tsai-Wu failure index is greater than or equal to 1. For accuracy, the results were evaluated at the Tsai-Wu failure index ranging between 1 and 1.1.

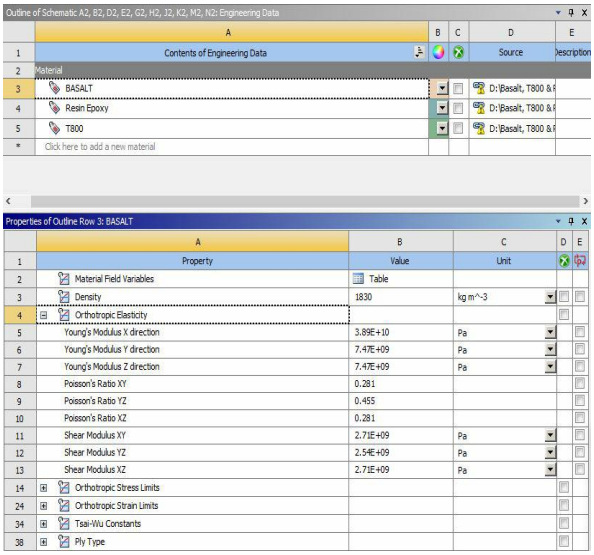

Figure 5: Engineering data module in ANSYS.

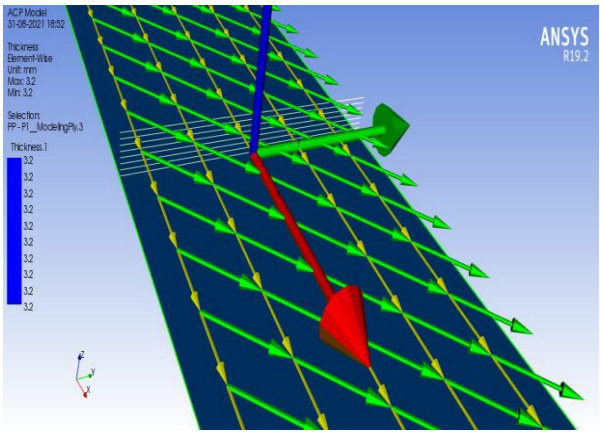

Figure 6: Fibre orientation in ANSYS ACP.

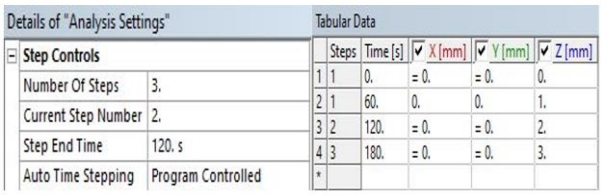

Figure 7: Time-steps in ANSYS Mechanical.

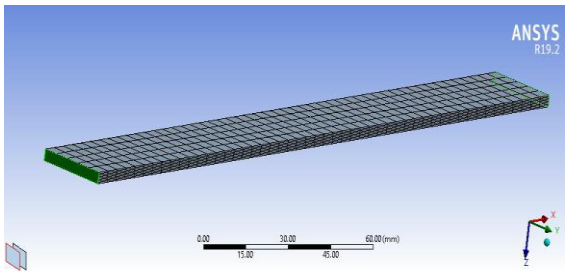

Figure 8: Meshed model with double displacement boundary condition ready for tensile loading in ANSYS

3. Results and Discussion

The results of static tests of these laminates are in line with the objectives of this paper. The FE results for tensile, compression, flexure, interlaminar, and in-plane shear tests have been evaluated and compared with the experiments. Since specimen C1, a pure carbon laminate is an industry standard composite material compared to the novel nature of basalt fibre, it served as a reference to compare the strength of other specimen configurations. The ratio of the strength of each specimen to that of specimen C1 was evaluated for FEA as well as experimental findings to validate the nature of FEA results.

3.1. Tensile Strength Evaluation

Table 3 shows the tensile test results comparison between FEA and the experimental tensile test. Similarly, the ratio of tensile strength of individual specimens with respect to pure carbon reference specimen C1 indicating the variation in tensile strength for both FEA results, and experimental findings is represented graphically. Figure 9 shows the comparison plot of these ratios. Pure carbon reference specimen C1 as anticipated produced the best results. FEA results showed that specimens C2 and B2, having a ratio of 0.99 and 0.98, resulted in strength near reference specimen C1 which indicates a good stacking sequence. Specimen B1, the pure basalt specimen having a ratio of 0.84 produced a poor overall resistance to static loads. In tension, specimens C4 and B4 which have only four layers of 0° plies attained minimum strength. Placing a ±45° layer on the outer side causes a decrease in the tensile strength of hybrid composites. Despite the deviations, the variation in the ratio of FEA results is akin to that of the experimental findings as evident from Figure 9. The discrepancies and deviations are commonly discussed in section 3.6. Figure 10 shows the sample ANSYS failure contour plot for the best-stacked basalt/carbon (C2). Inner layers fail when the failure index marginally exceeds 1.

Table 3: Tensile test results

Specimen	Tsai-Wu failure index	Experimental tensile strength (MPa)	FEA tensile strength (MPa)	FEA/Experimental ratio
C1	1.014	625	962.3	1.54
C2	1.004	591	956.4	1.62
C3	1.009	539	932.3	1.73
C4	1.004	527	869.4	1.65
B1	1.002	482	808.5	1.68
B2	1.007	554	943.8	1.70
B3	1.007	509	884.3	1.74
B4	1.007	499	889.8	1.78

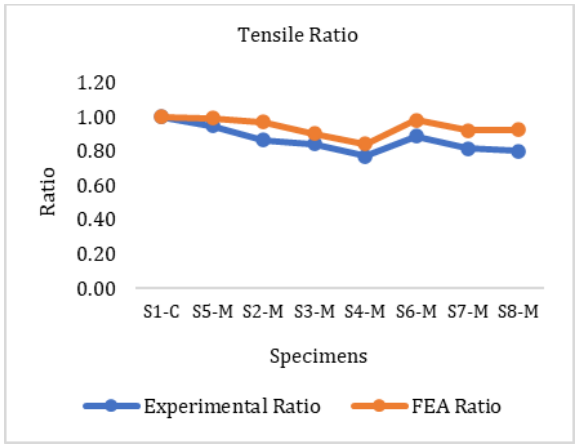

Figure 9: Tensile Test Ratio Plot for all Specimens.

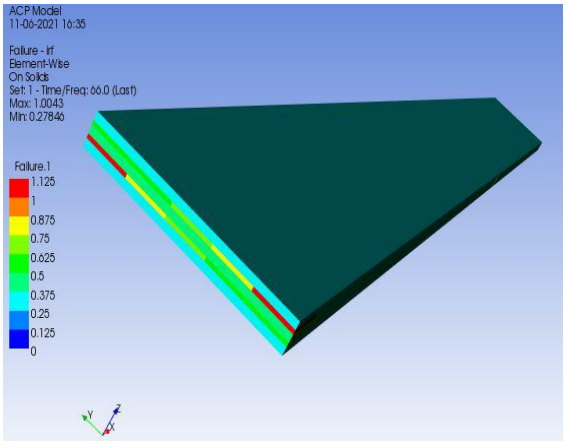

Figure 10: Tensile Test Results of Specimen C2.

3.2. Compression strength evaluation

Table 4 shows the compression test results comparison between FEA and the experimental compression test. Tsai-Wu failure index considered during the FEA is also listed. Similarly, the ratio of compressive strength of individual specimens with respect to pure carbon reference specimen C1 (benchmark laminate) indicating the variation in compressive strength for both FEA results, and experimental findings is represented graphically. Figure 11 shows the comparison plot of these ratios. In compression test simulation, specimens C3 (Figure 12) and B3 were concluded to be optimal because they produced a better response to compressive loads as evident from Table 4, and displayed lesser deviation with a ratio of 0.96 and 0.93 from the pure carbon reference specimen C1. The selection of specimens C3 and B3 can also be adduced by the fact that their configurations are mirror images of each other as mentioned in Table 2. In spite of the deviations, the fall in the ratio of FEA results for specimens C3 and B3 is similar to the experimental findings.

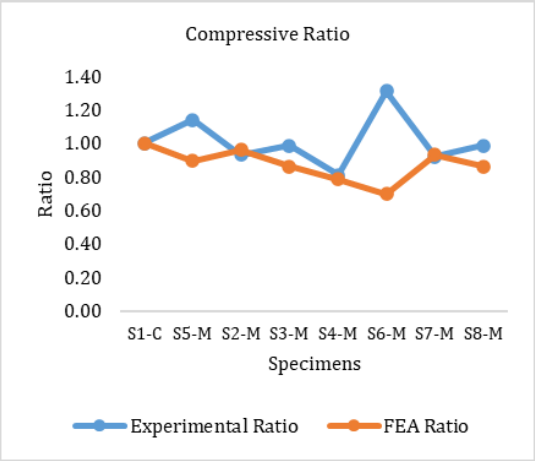

Figure 11: Compression test ratio plot.

3.3. Flexural strength evaluation

Table 5 shows the flexure test results comparison between FEA and experimental flexure tests. The Tsai-Wu failure index considered during the FEA is also listed. The ratio of flexural strength of individual specimens with respect to pure carbon reference specimen C1 indicating the variation in flexural strength for both FEA results and experimental findings is represented graphically. Figure 13 shows the comparison plot of these ratios. The pure carbon specimen C1 showed rapid and steep load rise, producing the highest flexural strength. The flexural strength of hybrid laminates with carbon fibres at the outer layers was higher than hybrid laminates with carbon fibres embedded in the middle layers, particularly for FEA. Results of specimen C2 were found to have a ratio of 0.93 with respect to pure carbon laminate. This is due to the higher strength of four carbon fibre layers which bears most of the applied load when placed at the outer side of the laminates. C2 produced flexural strength equal to the pure carbon laminate from the experimental findings and hence concluded as the optimal specimen for the flexural test. Figure 14 shows the specimen C2 failure contour.

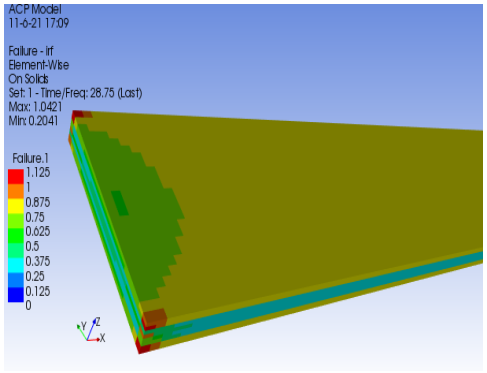

Figure 12: Compression test results of specimen C3.

Table 4: Compression test results.

Specimen	Tsai-Wu failure index	Experimental compression strength (MPa)	FEA compression strength (MPa)	FEA/Experimental ratio
C1	1.005	425	841.5	1.98
C2	1.021	485	751.5	1.55
C3	1.009	451	807.9	1.79
C4	1.007	445	726.3	1.63
B1	1.004	361	661.5	1.83
B2	1.008	473	585.1	1.24
B3	1.002	435	783.1	1.80
B4	1.003	429	724.2	1.69

Table 5: Flexural test results.

Specimen	Tsai-Wu failure index	Experimental-flexural strength (MPa)	FEA- flexural strength (MPa)	FEA/experimental ratio
C1	1.05	621	653.8	1.05
C2	1.1	589	609.4	1.03
C3	1.01	540	483.1	0.89
C4	1.07	521	572.7	1.10
B1	1.03	478	366.7	0.76
B2	1.09	538	401.7	0.75
B3	1.06	503	480.6	0.96
B4	1.02	492	397.9	0.81

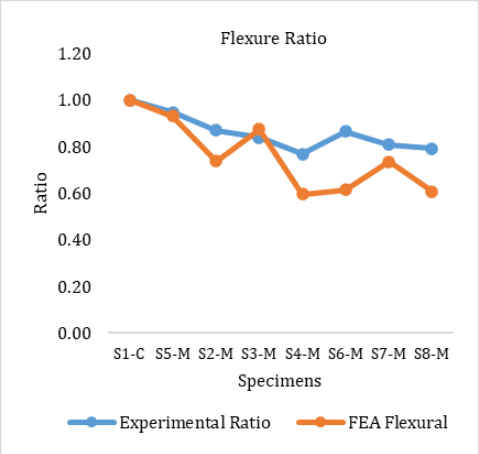

Figure 13: Flexure test ratio plot.

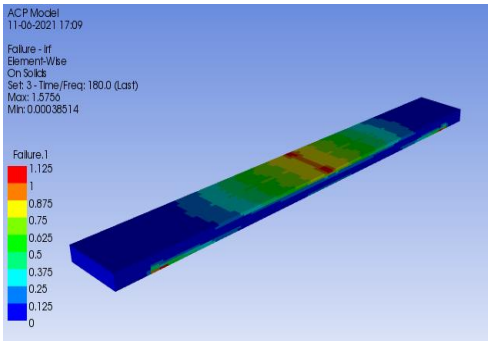

Figure 14: Optimal flexural specimen C2 results

3.4. Interlaminar shear strength evaluation

Table 6 shows the interlaminar shear stress (ILSS) test results comparison between FEA and experimental tests. The Tsai-Wu failure index considered during the FEA is also listed. The ratio of interlaminar shear strength of individual specimens with respect to pure carbon reference specimen C1 indicating the variation in interlaminar shear strength for both FEA results and experimental findings is represented graphically. Figure 15 shows the comparison ratio plot of both the test evaluations. Specimens C2 and C3 having a ratio of 0.95 and 0.92 respectively produced better interlaminar shear strength than their counterparts. This could be attributed to the fact that most of the transverse load was accosted by the fibres arranged perpendicular to the line of action of the applied load. Although C3 produced the same reduction in ratio as that of specimen C2, it was discarded as the optimal specimen based on a higher deviation from experimental findings. Figure 16 shows the failure contour of specimen C3, where the outer layers (carbon) are failing. This shows that basalt and carbon are no different for interlaminar shear related applications. The deviations in subsequent specimens obtained are discussed in section 3.6.

Table 6: Interlaminar shear test results

Specimen	Tsai-Wu failure index	Experimental interlaminar strength (ILSS)(MPa)	FEA - interlaminar shear strength (ILSS) (MPa)	FEA/experimental ratio
C1	1.08	21.8	17.3	0.79
C2	1.04	20.4	16.5	0.81
C3	1.1	22.9	15.9	0.69
C4	1.1	21.5	13.3	0.62
B1	1.06	24.3	12.7	0.52
B2	1.07	22.7	15.2	0.67
B3	1.05	16.1	14.1	0.88
B4	1.06	14.7	11.3	0.77

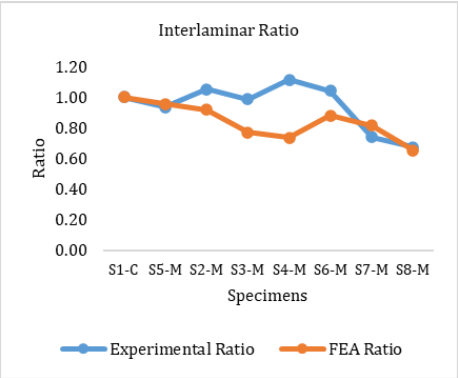

Figure 15: Interlaminar shear strength ratio plot.

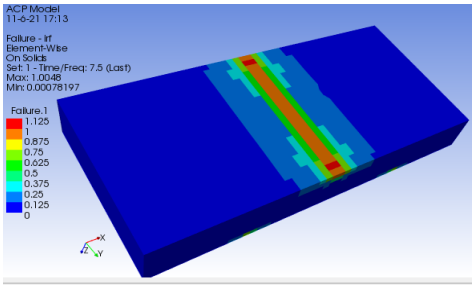

Figure 16: Best Interlaminar shear specimen C3.

3.5. In-plane shear strength evaluation

Table 7 shows the in-plane shear test results comparison between FEA and the experimental shear test. The Tsai-Wu failure index considered during the FEA is also listed. The ratio of in-plane shear strength of individual specimens with respect to pure carbon reference specimen C1 indicating the variation in in-plane shear strength for both FEA results and experimental findings is represented graphically. Figure 17 shows the comparison plot of in-plane shear strength ratios when compared with pure carbon laminate. Further for in-plane shear, specimen C2 having a ratio of 1.75 produced an in-plane shear strength response significantly greater than reference specimen C1. A similar observation was recorded for experimental findings where the ratio increased to 1.77. Both the ratios indicated the same rise as seen in Figure 17 where it is also evident that both FEA results and experimental findings were following a similar pattern. Figure 18 shows the sample in-plane shear failure contour of specimen C2.

Table 7: In-plane shear results.

Specimen	Tsai-Wu failure index	Experimental shear strength (MPa)	FEA results for in-plane shear strength (MPa)	FEA/experimental ratio
C1	1.004	17.8	16.6	0.93
C2	1.003	31.5	29.2	0.93
C3	1.004	27.6	19.2	0.70
C4	1.008	23.2	20.2	0.87
B1	1.011	15.2	13.6	0.89
B2	1.014	29.4	21.6	0.73
B3	1.002	25.1	24.7	0.98
B4	1.006	24.3	33.0	1.36

Table 8: Specimen C2 ratio

Test	Specimen C1 (Reference)	Specimen C2	Ratio = C2/C1
Tensile strength	962.3 MPa	956.4 MPa	0.99
Flexural strength	662.8 MPa	609.4 MPa	0.92
Interlaminar shear strength	17.8 MPa	16.5 MPa	0.93
In-plane shear strength	16.6 MPa	29.2 MPa	1.77

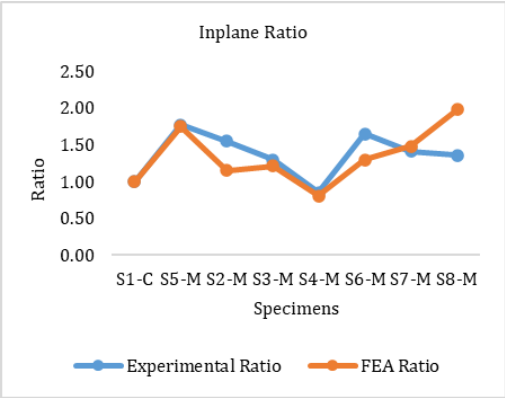

Figure 17: In-Plane shear strength ratio plot.

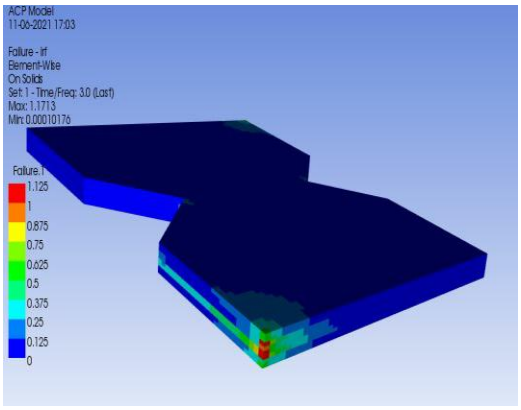

Figure 18: Best In-plane shear strength specimen C2.

3.6. Summary

On evaluating the result of static tests, it was observed that specimens C2 and B2 produced strength greater than most of the other specimens in the majority of the tests. An explanation might be the configurations of specimens C2 and B2 which are mirror images of each other when viewed about the plane of symmetry. While specimen B2 did offer promising results for interlaminar and in-plane shear tests with a ratio of 0.88 and 1.59 compared to pure carbon, it was discarded candidate for optimal specimen based on poor tensile and flexural response compared to specimen C2. From the above discussion, it can be summarized that specimen C2 produced an in-plane shear strength (29.2 MPa) significantly greater than reference pure carbon specimen C1 (16.2 MPa). Moreover, tensile, flexural, and interlaminar shear strength responses of specimen C2 are almost equal to the reference pure carbon specimen C1 as evident from the comparison ratio table (Table 8). Thus, from this analysis, it can be inferred that specimen C2 is the optimal specimen.

Using specimen C2 as a substitute for pure carbon not only provides better strength but also reduces the material cost. The percentage of savings by using basalt instead of carbon fibre is given by the equation below:

$$\text{Saving \%} = \frac{\text{Difference between cost of basalt fibre and carbon fibre per m2}}{\text{Cost of carbon fibre per m2}} \times 100 \quad \text{(Eq.2)}$$

$$\text{Saving \%} = \frac{(26.92 - 16.15)\text{USD}}{26.92\ \text{USD}} \times 100 = 40\%$$

3.7. Discussion for Deviations

1. Differences were observed between ANSYS simulations and experimental findings which can be attributed to the composite curing process as evident from the works of Kumbhare et al. [26]. The composite curing process leads to various chemical interactions like cross-linking of fibres as well as structural distortions in the laminate, inducing residual stresses which cause premature failures in composites.

2. The experimental findings tabulated failure on basis of de-bonding (fibre fracture) or delamination (ply separation) theories. In practice, a resin was used to bind the layers together which made delamination, a probable cause of failure when the interfacial strength was exceeded. However, while performing simulations, since it was a solid composite model, the ANSYS solver fixed the layers above each other which made debonding the only mode of failure.

3. In contrast to traditional experiments where a resin is used to bind two layers, while performing simulations, combined properties of resin and fibre were imparted to a single layer in order to account for the effect of resin followed by the other layers which were modeled in the same way.

4. ANSYS Mechanical works on Inverse Reserve Factor (IRF) plot that divides the ultimate strength by the von Mises equivalent stress at each node. Therefore, when IRF > 1 the part was considered to have failed, and when IRF < 1 the part has not failed.

4. Conclusion and Future Work

Basalt, although a newcomer, presents immense potential to be utilized especially in today's evolving world and its expectations in the field of hybrid composites. Based on the observations and discussion of the results, the major outcomes of the work are as follows:

1. It is established that embedding the basalt fibre layer in the inner part or using carbon fibre in the outer layers of the composite has led to the production of composite with strength in proximity to the unidirectional pure carbon specimen C1.

2. The optimal basalt/carbon stacking sequence based on the results was found to be specimen C2 $[02C/\pm45B/0B]_S$. The comparison table showed that specimen C2 can be a decent

substitute for pure carbon laminates. Apart from strength advantage, the work also demonstrates that substituting basalt fibre in a 4:4 ratio with carbon fibre provides a substantial cost reduction of around 40%.

3. The paper also presented deviations in strength evaluation between experimental and FE analysis which was varying for different tests. Tensile tests showed an average variation of 60%, while compression tests' average variations were 70%. Meanwhile, the variations in flexure, interlaminar shear, and in-plane shear tests were around 15%, 20%, and 12%, respectively.

As part of the future scope, a parametric study to examine the influence of different parameters like specimen geometry, newer materials, and evaluation of hole pattern arrangement can be conducted.

5. Acknowledgments

The authors would like to thank Manipal University Jaipur for providing space and software facilities for this research work.

References

[1] Wang, Y., Zhang, T., Zhou, L., Yan, C., Wang, N., Gu, J. and Chen, L., 2019. Damage characteristics of basalt fiber reinforced mortar under compression evaluated by acoustic emission. Materials Testing, Vol. 61 (Issue 4), pp. 381-388. https://doi.org/10.3139/120.111332

[2] Sakthivel, M., Jenarthanan, M. and Raja, P., 2019, Mechanical properties, degradation and flue gas analysis of basalt and glass fiber reinforced recycled polypropylene. Materials Testing, Vol. 61 (Issue 6), pp. 579-583. https://doi.org/10.3139/120.111358

[3] Richard Parnas, Montgomery Shaw, Qiang Liu, Basalt Fibre Reinforced Polymer Composites, *The New England Transportation Consortium*, Project No. 03-7, August 2007, DOI:

[4] Kunal Singha, A Short Review on Basalt Fibre, *International Journal of Textile Science,* vol. 1 no. 4 pp: 19-28, DOI: 10.5923/j.textile.20120104.02

[5] Mingchao, W. et al., 2008. 'Chemical Durability and Mechanical Properties of Alkali-proof Basalt Fiber and its Reinforced Epoxy Composites', Journal of Reinforced Plastics and Composites, 27(4), pp. 393–407. DOI: 10.1177/0731684407084119.

[6] Czigány, T., 2006. Special manufacturing and characteristics of basalt fiber reinforced hybrid polypropylene composites: Mechanical properties and acoustic emission study. Composites Science and Technology. https://doi.org/10.1016/j.compscitech.2005.07.007

[7] Aslan, M. and Kaymaz, E., 2020. Characterization of thick carbon/basalt hybrid fiber polyester composites with graphene nanoplatelets. Materials Testing, Vol. 62 (Issue 1), pp. 12-18. https://doi.org/10.3139/120.111457

[8] Khalili, S. M. R., Daghigh, V. and Eslami Farsani, R., 2011. 'Mechanical behavior of basalt fiber-reinforced and basalt fiber metal laminate composites under tensile and bending loads', Journal of Reinforced Plastics and Composites, 30(8), pp. 647–657. 10.1177/0731684411398535.

[9] Abdalla, J.A., Hawileh, R.A., Rasheed, H.A., 2022. Behavior of Reinforced Concrete Beams Strengthened in Flexure using Externally Bonded Aluminium Alloy Plates. Procedia Structural Integrity. https://doi.org/10.1016/j.prostr.2022.01.134

[10] Naser, M.Z., Hawileh, R.A., Abdalla, J.A., 2019. Fiber-reinforced polymer composites in strengthening reinforced concrete structures: A critical review. Engineering Structures. https://doi.org/10.1016/j.engstruct.2019.109542

[11] Maxineasa, S.G., Taranu, N., 2018. Life cycle analysis of strengthening concrete beams with FRP. Eco-Efficient Repair and Rehabilitation of Concrete Infrastructures. https://doi.org/10.1016/b978-0-08-102181-1.00024-1

[12] El Refai, A., Alnahhal, W., Al-Hamrani, A., Hamed, S., 2022. Shear performance of basalt fiber-reinforced concrete beams reinforced with BFRP bars. Composite Structures. https://doi.org/10.1016/j.compstruct.2022.115443

[13] Gencel, O., Nodehi, M., Yavuz Bayraktar, O., Kaplan, G., Benli, A., Gholampour, A., Ozbakkaloglu, T., 2022. Basalt fiber-reinforced foam concrete containing silica fume: An experimental study. Construction and Building Materials. https://doi.org/10.1016/j.conbuildmat.2022.126861

[14] Yang, C., Liu, Z., Tong, X., Guo, L., Miao, S., Jiang, L., Li, Y., Li, H., Liu, C., 2022. Effects of raw material homogenization on the structure of basalt melt and performance of fibers. Ceramics International. https://doi.org/10.1016/j.ceramint.2022.01.049

[15] Zheng, Y., Sun, D., Feng, Q., Peng, Z., 2022. Nano-SiO2 modified basalt fiber for enhancing mechanical properties of oil well

cement. Colloids and Surfaces A: Physicochemical and Engineering Aspects. https://doi.org/10.1016/j.colsurfa.2022.128900

[16] Chandrasekar, M., Ishak, M.R., Jawaid, M., Sapuan, S.M., Leman, Z., 2018. Low velocity impact properties of natural fiber-reinforced composite materials for aeronautical applications. Sustainable Composites for Aerospace Applications. https://doi.org/10.1016/b978-0-08-102131-6.00014-1

[17] Mengal, A N, *Fatigue Life prediction of Basalt-Carbon/Epoxy Hybrid Laminated Composite for Wind Turbine Rotor Blades*, PhD thesis, Universiti Teknologi Petronas, August 2016, DOI: http://utpedia.utp.edu.my/18306/

[18] Di Ludovico, M., Prota, A., Manfredi, G., 2010. Structural Upgrade Using Basalt Fibers for Concrete Confinement. J. Compos. Constr. https://doi.org/10.1061/(asce)cc.1943-5614.0000114

[19] Gao, L., Adesina, A., Das, S., 2021. Properties of eco-friendly basalt fibre reinforced concrete designed by Taguchi method. Construction and Building Materials. https://doi.org/10.1016/j.conbuildmat.2021.124161

[20] Afrathim, A., Karuppanan, S., Patil, S.S., 2021. Burst strength analysis of thin composite pressure vessels. Materials Today: Proceedings. https://doi.org/10.1016/j.matpr.2021.02.808

[21] ASTM D3039 / D3039M-17, Standard Test Method for Tensile Properties of Polymer Matrix Composite Materials, ASTM International, West Conshohocken, PA, 2017, www.astm.org

[22] ASTM D6641 / D6641M-16e2, Standard Test Method for Compressive Properties of Polymer Matrix Composite Materials Using a Combined Loading Compression (CLC) Test Fixture, ASTM International, West Conshohocken, PA, 2016, www.astm.org

[23] ASTM D7078 / D7078M-20e1, Standard Test Method for Shear Properties of Composite Materials by V-Notched Rail Shear Method, ASTM International, West Conshohocken, PA, 2020, www.astm.org

[24] ASTM D2344 / D2344M-16, Standard Test Method for Short-Beam Strength of Polymer Matrix Composite Materials and Their Laminates, ASTM International, West Conshohocken, PA, 2016, www.astm.org

[25] ASTM D7264 / D7264M-21, Standard Test Method for Flexural Properties of Polymer Matrix Composite Materials, ASTM International, West Conshohocken, PA, 2021, www.astm.org

[26] Kumbhare, N., Moheimani, R., Dalir, H., 2021. Analysis of Composite Structures in Curing Process for Shape Deformations and Shear Stress: Basis for Advanced Optimization. J. Compos. Sci. https://doi.org/10.3390/jcs5020063

[27] ANSYS, Inc. ANSYS Composite PrepPost Users Guide [Online] Available at: https://www.scribd.com/document/308210468/ANSYS-Composite-PrepPost-Users-Guide [accessed: March 04, 2021]